AUT Journal of Electrical Engineering
10.22060/EEJ.2026.25662.5978

Integration of Active Boost Step up Converter with Optimized ANN in PV Based UPFC System for Improved Grid Stability

Thirunavukkarasu Subramanian[1], Arulkumar Chinnusamy[2], Satheeshkumar Rajendran[3*], Nivetha Rathinam[4]

[1]Associate Professor, Department of Electrical and Electronics Engineering, Paavai Engineering College, Namakkal - 637018, India.
[2]Associate Professor, Department of Electrical and Electronics Engineering, Paavai Engineering College, Namakkal - 637 018, India.
[3*]Assistant Professor, Department of Electrical and Electronics Engineering, Paavai Engineering College, Namakkal - 637018, India.
[4]PG Student, Department of Electrical and Electronics Engineering, Paavai Engineering College, Namakkal - 637 018, India.
*Corresponding author E-mail: satheesh2811@gmail.com

Uncorrected Proof

Abstract:

The growing proportion of Renewable Energy Sources (RESs) poses significant challenges for modern grids, particularly in terms of power flow stability, voltage management, and power quality. Traditional UPFCs rely on grid-connected DC link limiting their ability to operate sustainably and adapt flexibly to changing system conditions. To overcome such issues this research proposes a Photovoltaic (PV)-powered UPFC system incorporated with a Coupled Inductor (CI) Active Boost Step Up Converter to provide a stable high-gain supply to DC link. An advanced control strategy is introduced to extract maximum power using Artificial Neural Network (ANN) based Sharp belly Fish Optimization Algorithm (SFO) under varying environmental conditions. The series converter is connected through a transformer operates as a dynamic voltage compensator and shunt converter combined with an LC filter performs DC voltage regulation. MATLAB/Simulink validation shows better performance in terms of reduced Total Harmonic Distortion (THD), faster transient response, and enhanced steady-state voltage control as compared to traditional UPFC techniques. The obtained efficiency is around 94% and tracking efficiency is 99.9% with reduced THD 0.75%.

Keywords:

PV, ANN-MPPT Controller, SFO, CI-Active boost step-up converter, PI controller.

1. Introduction

Fossil fuels have been used for many decades to meet the world's energy growing demands. However, fossil fuels are being depleted and contribute to environmental pollution through emission of green house gases [1]. PV experiences rapid growth with increased global investment in renewable energy and modern techniques often incorporate with proper system design, and maintenance [2]. PV has more benefits including longevity, safety, and non-pollutant. However, the production of power is random and instable due to climate, spike, and sunshine time then it generates low power [3]. In order to increase PV output DC-DC converters are necessary in [4] Non-isolated converters with high power density, for microgrid application. The merits of this converter include reduced voltage stress across components, high robustness, and minimized conduction losses. Nevertheless, high instantaneous current flowing through passive element results in increased power losses [5]. boost converter for PV system with greater efficiency and simple structure. It has minimized fluctuations, compact and light weight, flexible voltage control. However it exhibits dangerous conduction losses, switching stress, unnecessary input current ripples, and high cost [6-7].Interleaved converters for PV applications which has less ripples in output voltage, high performance, minimized ripples, faster transient response, scalability, improved reliability. However it experience circuit complexity, higher cost, and reduced efficiency [8].Quadratic boost converters with high voltage gain for grid applications improve durability, and reliability, ensuring the longevity, enhanced power density and soft switching capability. Nevertheless the converter maintains a limited efficiency range and has high copper loss, and increases the complexity of the circuit [9-10].Interleaved quadratic converters for grid application which has enhanced power quality, and compensate for microgrid's power management. It has extremely low voltage stress, and condensed switching losses. Nevertheless voltage gain is enhanced, it needs several count of elements, increased transformer turn ratio, and THD level is high [11-12]. Though the converters provide many benefits but it

Uncorrected Proof

10.22060/EEJ.2026.25662.5978

also face certain limitations, to overcome these issues and ensures proper performance to increase the PV low voltage MPPT controllers are required.

A Fuzzy Logic controller for a PV system for extracting maximum power underneath varying conditions. It has an outstanding performance in unexpected fluctuations in operating temperature of PV module, fast and stable response, cost effective. However, it faces low convergence, design complex and high computational [13]. P&O MPPT controller in real-time investigation of enhancing voltage for PV system. It ensures the system to functions at maximum efficiency, minimized oscillations, and lower cost. Although it suffers from slow convergence, power losses, and poor tracking performance [14].The MPPT controller exhibits some limitations and to succeed it optimization is required for proper tuning of controller parameters. Genetic Algorithm-MPPT controller for grid-PV system under varying conditions. It exhibits robustness, improved system reliability, efficiency, and adaptability. However it's computationally intensive is slow to converge and requires proper tuning [15].PSO-MPPT controller for, which has high tracking efficiency, robustness, reliability, fault tolerance and fast convergence. However it often got stuck in local optima, computational complexity, fluctuations, and low cost [16].ACO-MPPT algorithm is highly effective in extracting maximum power due to strong searching capability. It demonstrates excellent tracking performance, minimized chances of being trapped in local minima. However despite these advantages the algorithm relatively suffer from slow convergence, affecting steady state efficiency [17-18].

Henceforth the limitations overcome by this proposed system of CI-Active boost converter with SFO-ANN-MPPT algorithm for stabilized UPQC system.

2. Recent Works

Aman Gautamet *et al* [2022] [19] have proposed STATCOM which is a shunt compensation device, for reactive power compensation and voltage regulation in power systems. It effectively mitigates

Uncorrected Proof

10.22060/EEJ.2026.25662.5978

fluctuations, and remains in a steady state voltage by dynamically controlling the exchange of reactive power with grid. It exhibits fats dynamic response, reduced harmonic distortion, and more compact size. However, it offers installation cost is relatively high, limited capability of real power compensation, as switching losses, and requires additional control.

P.V.V. Satyanarayana *et al* [2022] [20] have demonstrated DSTATCOM as an effective solution for mitigating harmonic distortion by compensating all current related power quality issues in power distribution system. It significantly reduces, reduced harmonic components, minimized number of elements and ensures reliable and stable operation. However, imbalanced power flow results in increased conduction loss neutral current effects, and elevated switching stress which adversely affects the system lifespan.

Ghareeb Moustafaet *et al* [2023] [21] have introduced SVC to maximize early energy savings in power losses. It exhibits superior performance by reducing power losses, lower harmonic distortion, improved power factor correction, and enhanced overall system stability. Although the lowest voltage at the respective loading range an improved system still it exhibits certain limitations particularly related to voltage imbalance.

Nguyen Nhan Bonet *et al* [2022] [22] have offered TCSC to enhance power system by improving systems reliability, minimizing installation cost, and offer through its dynamic operating capability. However, when the transmitted power exceeds the limit, it leads to overloading and potentially causing damage to the electrical system.

Amirreza Bahadori1 *et al* [2022] [23] have developed non-isolated converter that is used for reducing voltage stress in power switches and maintain stable voltage. It exhibits high voltage gain, increased system stability, reduced fluctuations and low number of components. However it has design complexity, increased converter size and high cost.

Uncorrected Proof

10.22060/EEJ.2026.25662.5978

2-1- Contribution of the work:

To deliver a steady high-gain DC-link voltage and enhance grid stability and power quality, the proposed work incorporates a PV-powered UPFC with an Active Boost Step-Up Converter. To accomplish effective solar energy extraction under varied irradiance circumstances, an optimised ANN-MPPT controller utilising the SFO algorithm is employed. For dynamic voltage compensation, the UPFC uses a series converter for DC-link voltage regulation and reactive power support, it employs a shunt converter with an LC filter.

The paper presents introduction in section I, Recent works are presented in section II, proposed system description and modeling in Section III and result discussion is explained in section IV and section V defines conclusion.

3. Proposed System Description

The block diagram is revealed in Fig. 1.The proposed system combines PV with UPQC structure to ensure stable and high quality power to load. The UPQC structure consist of series and shunt converter for mitigating voltage and current disturbances in the distribution network. A DC-link serves as an energy buffer and provides the necessary power for shunt and series converters. The series converter connected through a series transformer that operates as a dynamic voltage compensator. Furthermore the shunt converter is attached in parallel with load through shunt transformer and LC filter that performs current compensation and DC-link voltage regulation. In order to maintain a stable voltage regulation in DC-link and provides continuous energy support an integrated PV system is used as a primary energy source with CI- Active Boost step-up converter.

Uncorrected Proof

AUT Journal of Electrical Engineering
10.22060/EEJ.2026.25662.5978

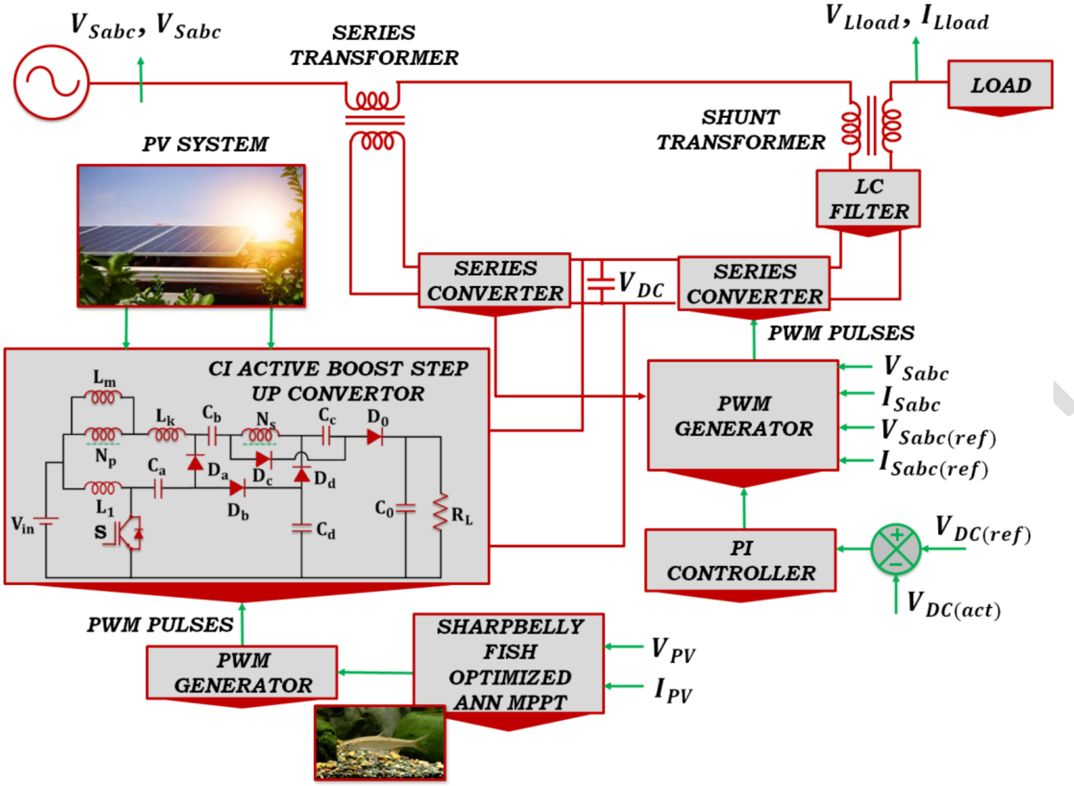

Fig. 1. Proposed block diagram

Additionally an SFO-ANN MPPT algorithm is employed to extract maximum power from PV under varying condition and to regulate DC output. Finally the compensated voltage is delivered via an LC filter to remove switching harmonics being delivery to the load. Consequently the proposed system improves overall system efficiency and reliability and appropriate PI controller regulates DC-link voltage and ensures effective UPQC performance.

4. Proposed System Modelling:

4-1- PV System

PV module which alters solar energy into electricity and it usually consist of a single diode, resistor connected in series and shunt, photocurrent sources and solar irradiance, ambient temperature. The circuit for PV is given in Fig. 2.

10.22060/EEJ.2026.25662.5978

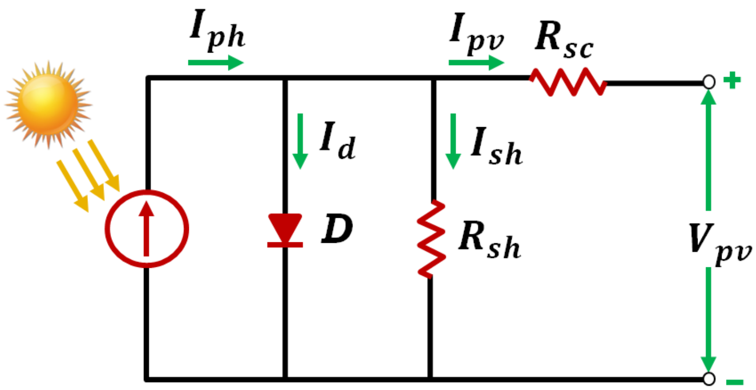

Fig. 2. PV circuit

VI characteristics of PV is expressed from photocurrent which is expressed by,

$$I_{pv} = I_{ph} - I_d - I_{sh} \tag{1}$$

$$I_d = I_s \cdot \left[exp\left(\frac{V_{pv} + I_{pv} \cdot R_{sc}}{A.k.T.act.N_s} \cdot q \right) - 1 \right] \tag{2}$$

$$I_{sh} = \frac{V_{pv} + I_{pv} \cdot R_{sc}}{R_{sh}} \tag{3}$$

Here N_s is the count of cells in parallel, R_{sh} is the shunt resistance, q is the charge, R_{sc} is the series resistance, I_{pv} denotes the photocurrent, I_d is the diode current, and subsequently various changes in parameters of PV module produce a dominant effects in output power from PV. To improve the output of PV, converters are essential to increase low voltage.

4-2- Coupled Inductor (CI) Active Boost Step up Converter

CI-active boost step up converter is a high efficiency DC-DC topology utilizing magnetic coupling used to achieve very high voltage gain. It often used to boost low voltage sources to greater voltage levels. The circuit is shown in Fig. 3.

Uncorrected Proof

10.22060/EEJ.2026.25662.5978

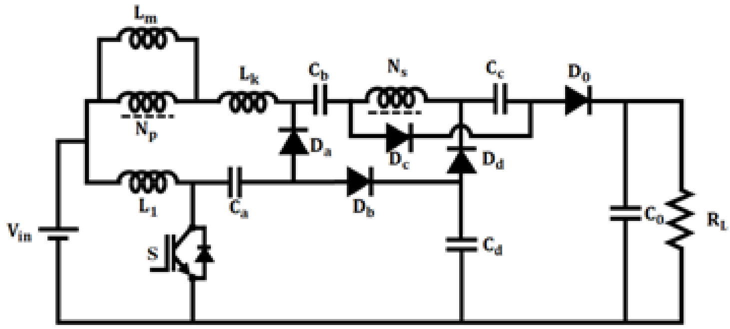

Fig. 3. Equivalent circuit

The circuit consist of a single switch, five diodes, and capacitors namely, C_a, C_b, C_c, C_o, two winding coupling inductor where L_k act as leakage inductance L_m as magnetising inductance, with a load resistance R_L. Two modes of operation takes place and the circuit is given in Fig. 4 for stage 1.

Mode 1:

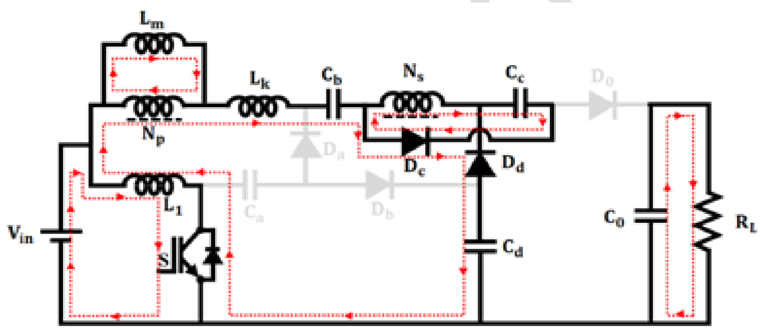

Fig. 4. Mode 1(switch ON)

In this stage, the input voltage is applied across the primary winding, when the switch is ON and D_c *and* D_d is active and inductor L_1 *and* L_m magnetized by input voltage and capacitor voltage. The capacitor C_o stores stable voltage and supply it to the load, which act as a sole component storing energy. The change in current is expressed as,

$$\frac{d_i}{dt} = \frac{V_{cc} + V_{Cd} - (n+1)V_{C_a} - nV_{in} - V_o}{n^2 L_K} \tag{4}$$

10.22060/EEJ.2026.25662.5978

Mode 2: During mode 2 switch is OFF, energy stored in the inductor and diode D_b and D_a, act as forward biased and the capacitor C_o deliver power to the load.

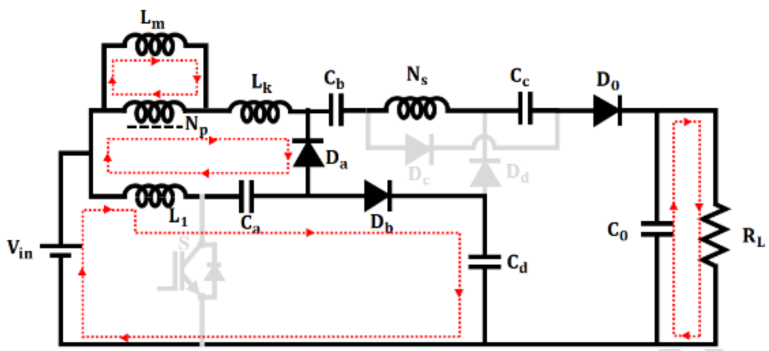

Fig. 5. Mode 2(switch OFF)

The leakage inductor control current is derived as,

$$\frac{d\left(i_{DC}+i_{DD}\right)}{dt}=\frac{V_{cc}-nV_{in}-\left(n+1\right)V_{ca}-V_{Cb}}{n^2 L_K} \tag{5}$$

Steady state analysis:

The magnetising inductor voltage is calculated by,

$$V_{L_M}=V_{in}+V_{C_a} \tag{6}$$

Output voltage from converter is,

$$V_o=\left(n+1\right)V_{Cb}+V_{cc}+V_{Cd}-nV_{in} \tag{7}$$

$$V_{Cd}=n\left(V_{in}+V_{C_a}\right) \tag{8}$$

Applying volt-second balance, capacitor voltage is determined as,

$$V_{C_a}=\frac{1}{\left(1-D\right)}V_{in} \tag{9}$$

$$V_{Cb}=\frac{1}{\left(1-D\right)^2}V_{in} \tag{10}$$

Uncorrected Proof

10.22060/EEJ.2026.25662.5978

$$V_{cc} = V_{C_a} + V_{Cb} + V_{Cd} \tag{11}$$

$$V_{cc} = \frac{(2-D)[1+n(1-D)]}{1-D} V_{in} \tag{12}$$

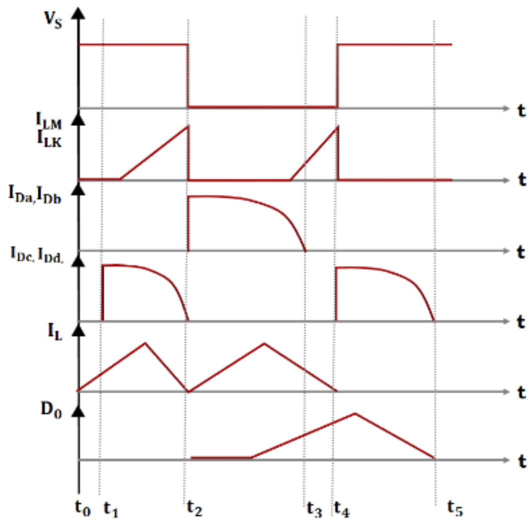

Fig. 6. Timing diagram

$$V_{Cd} = n\left(\frac{2-D}{1-D}\right) V_{in} \tag{13}$$

Maximum gain attained by the converter is given by,

$$\frac{V_o}{V_{in}} = \frac{1+(2-D)[1+n(2-D)}{(1-D)^2} \tag{14}$$

Voltage stress across switches is derived as,

$$V_S = V_{C1} = \frac{1}{1-D} V_{in} \tag{15}$$

Hence the converter provides a high voltage gain with minimized stress and to enhance the performance and regulate this converter output controllers are essential.

4-3- Sharpbelly-optimized ANN-MPPT controller

Uncorrected Proof

10.22060/EEJ.2026.25662.5978

An SFO-ANN MPPT controller utilizes an intelligent algorithm to enhance training and performance of ANN that controls DC-DC converter, it maximizes energy extraction under varying condition and the optimization reduces the training time of ANN and ensures hidden layers of neurons. ANN-MPPT structure is illustrated in Fig. 7.

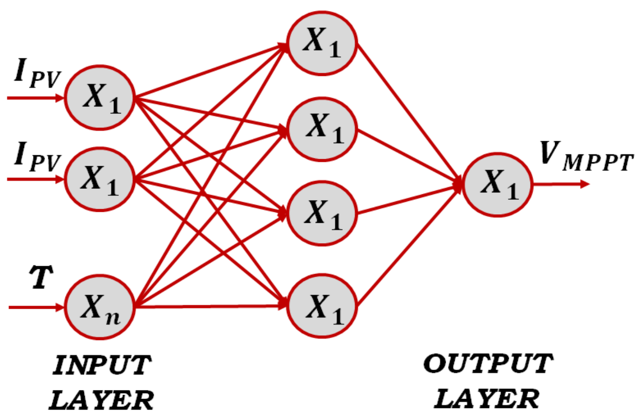

Fig. 7. ANN-MPPT structure

ANN network is motivated by living neurons. It also has the ability to perform MPPT under varying conditions. MPPT algorithm using neural network with feed forward multi-layer provides better response of ANN in extracting maximum power. These inputs are interconnected to neurons in the hidden layer where weighted sums and activation functions are applied to arrest the non-linear association among ecological conditions. The processed signals are transmitted into output neuron that predicts the optimal maximum power point voltage(V_{MPPT}).

Eventhough the controller extracts maximum power, it is unstable and parameters needs to be tuned properly. In order to optimize the controller parameters optimization is essential. The sharp belly is a trivial fish swimming in brackish water that displays a variety of natural group behavior in its usual habitat that bids rich inspirations for scheming swarm-optimization policies. It originates from scavenging and dodging behavior of Hemiculter leucisculus with obliging swimming way combination, and rapid dispersal under fears. The algorithm is computationally, well-organized with direct time difficulty in

Uncorrected Proof

10.22060/EEJ.2026.25662.5978

terms of population size, problem dimension, and iteration count. This optimization includes population initialization, swimming and gathering, Escape behavior, dispersal due to stagnation. The flowchart is illustrated in Fig. 8. The population size is N and P_f is probability of disturbance occurrence in the escape behaviour.

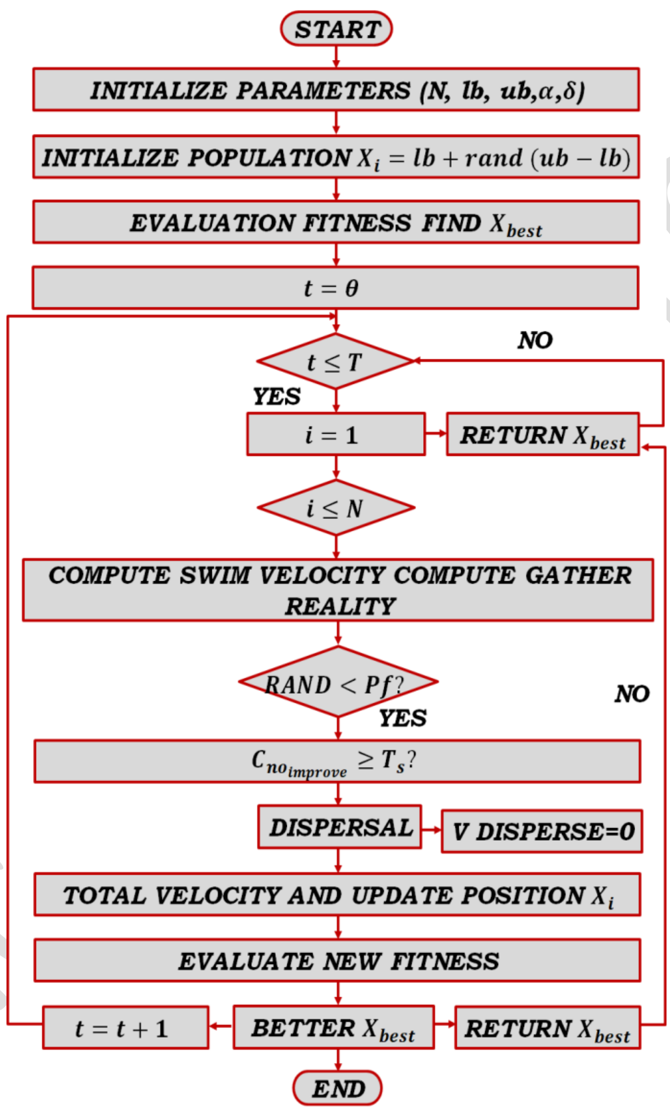

Fig. 8. Flowchart of SFO

Population initialization: the algorithm starts with initial population of individuals where positions are initially dispersed inside distinct limits, is defined as,

10.22060/EEJ.2026.25662.5978

$$X^{O} = rand\left(N,D\right).\left(ub-lb\right)+lb \tag{16}$$

Fitness function is represented by,

$$F^{t} = \left[f\left(X_{1}^{t}\right), f\left(X_{2}^{t}\right), \cdots f\left(X_{N}^{t}\right) \right]^{T} \tag{17}$$

Swimming behavior: inborn propensity of fish is remodeled to pursue the nutrient rich zones, with speed inversely proportional to its fitness value. The adaptive swimming step size is s_i^t.

$$V_i^{swim} = s_i^t \cdot rabd() \cdot \left(X_{best}^{t} - X_{1}^{t} \right) \tag{18}$$

Here, the swimming velocity component is V_i^{swim}.The current optimum global is represented by,

$$V_i^{gather} = \propto \cdot rand() \cdot \left(X_{best}^{t} - X_{i}^{t} \right) \tag{19}$$

Escape behavior: By rapidly changing direction, the fish strongly disturb their habitat, as mathematically described as,

$$V_i^{disturb} = \{ \delta \cdot N\left(0,1\right), if \ \ rand < P_f \quad o, \ otherwise \tag{20}$$

Where disturbance velocity is indicated by$V_i^{disturb}$, gathering velocity is denoted by V_i^{gather}, X_{best}^t denotes the best global position and V_i^{swim} signifies the swimming velocity .

Dispersal due to stagnation: It is an absence of development over a secure count of iterations to help individuals to seepage local optima.

Position inform: The active behaviour components is termed from addition of velocity of each fish,

$$V_i^{t} = V_i^{swim} + V_i^{gather} + V_i^{disturb} + V_i^{disperse} \tag{21}$$

Each fish update its position based on vector velocity as per feasible rule,

$$X_i^{t+1} = \min(\max\left(X_i^{t+1}, lb \right), ub \tag{22}$$

Uncorrected Proof

10.22060/EEJ.2026.25662.5978

The ease of application, modest presentation, making it a talented applicant for solving optimization issues. The overall computational complexity mainly arises from key pages such as population, initialization, fitness evolution, and position update.

4-4- PI Controller

PI controller removes sturdy state error, which combines proportional and integral actions control mechanism used to regulate system. The proportional term produces output which is directly proportional to current error. The block for PI controller is provided in Fig. 9.

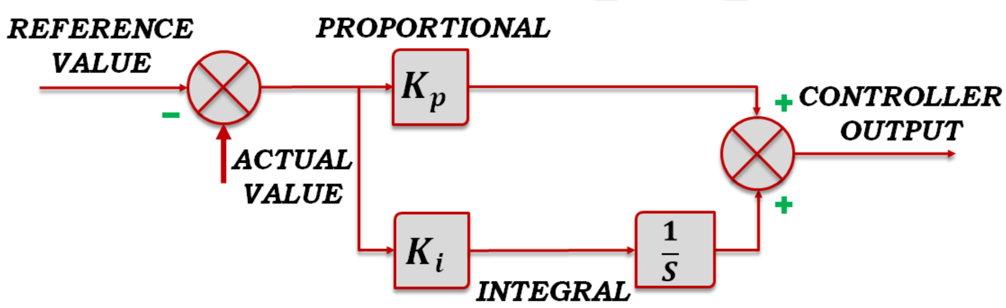

Fig. 9. PI controller block diagram

The transfer function of this controller is given by,

$$C(S) = K_P + \frac{K_I}{S} \tag{23}$$

Thus the controller ensures the system stability and by properly tuning the parameters effective disturbances are removed. Therefore the overall system enhances the power quality, increase voltage stability and power factor.

5. Result and Discussion

Uncorrected Proof

10.22060/EEJ.2026.25662.5978

The overall experimental results are validated using MATLAB/Simulink software which is used in various simulation, modelling and data analysis. The following table illustrates parameter specification.

Table 1. Parameter specification

Parameter	Rating
AC source	
Load Inductance	$10mH$
Load Resistance	100Ω
PV System	
Power rating	$25kW$
Open Circuit Voltage (V_{OC})	$37.25V$
Short Circuit Current	$8.95A$
No. of series panels	13
Count. of panels in parallel	3
Proposed converter	
L_1, L_k, L_m	$4.7mH$
C_a, C_b, C_c,C_d	22μF
C_{Out}	2200μF
Switching frequency	10kHZ

Case 1) 0 Amplitude

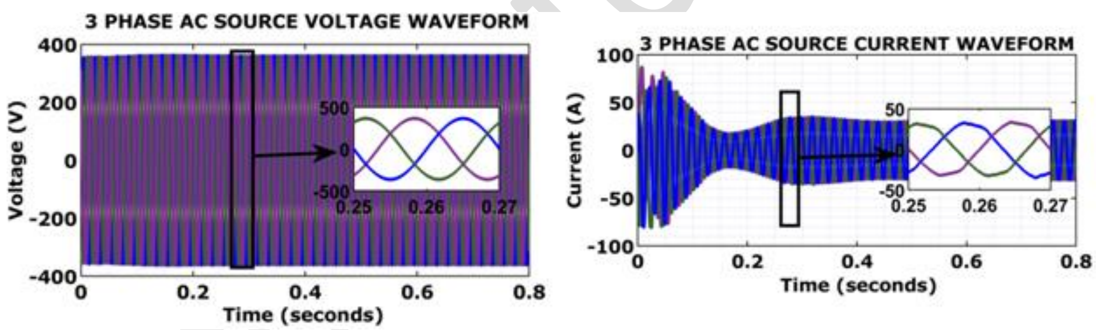

Fig. 10. Three phase AC source waveform

Fig. 10 illustrates three phase AC source waveform. The voltage stabilized at peak amplitude approximately $400V$with 50Hz. The current waveform displays transient behaviour at beginning and achieves $40A$ around $0.3s$.

10.22060/EEJ.2026.25662.5978

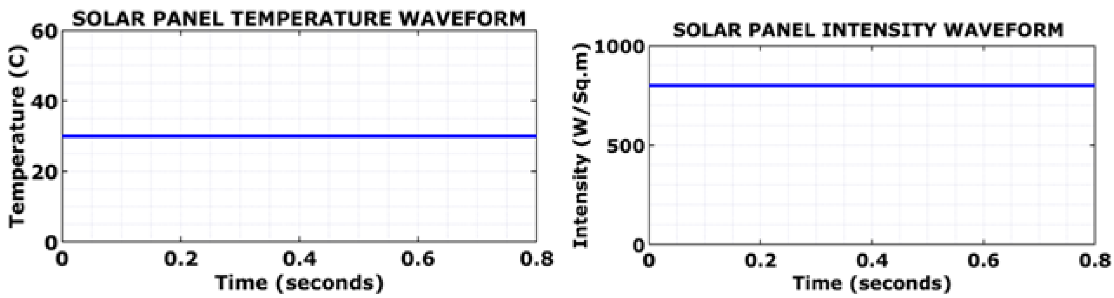

Fig. 11. Solar PV waveform

Fig.11 represents PV operating conditions over a time period around $0.8s$. The temperature remains constant throughout the entire period approximately $30°C$. The solar irradiance achieves $800wb/m^2$ indicating the system operating under stable environmental condition.

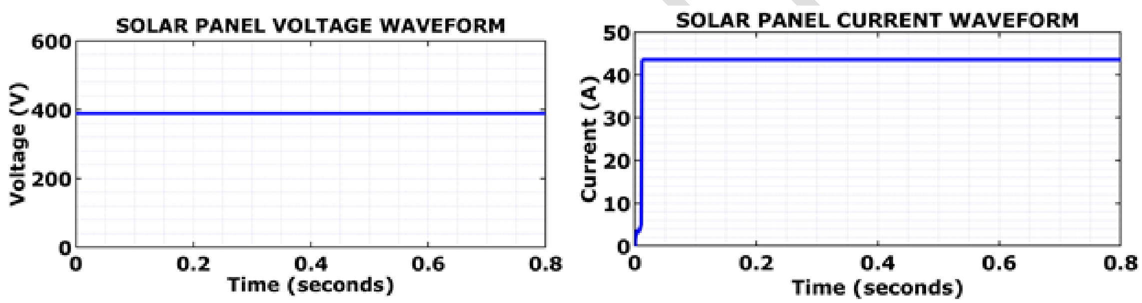

Fig. 12. Waveform of PV voltage and current

PV voltage and current characteristics is illustrated in Fig.12. The PV voltage gained about $390V$, and current reaches $47A$ approximately.

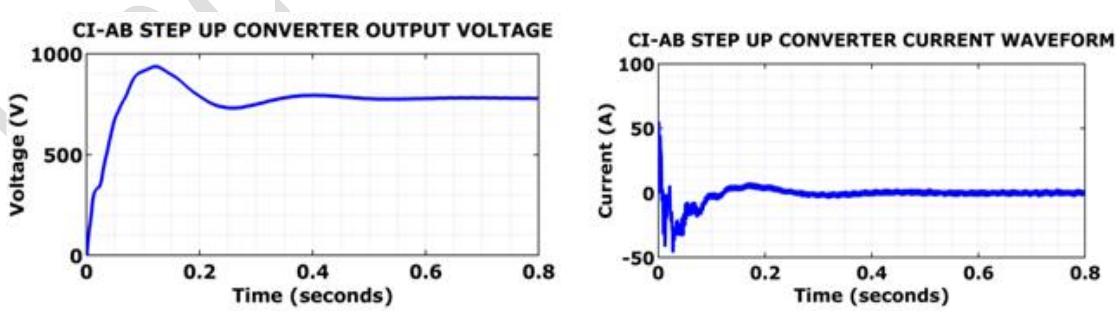

Fig. 13. Waveform of Converter input voltage and current

10.22060/EEJ.2026.25662.5978

Fig. 13 presents converter input graph, the converter output voltage is about $790V$. The voltage waveform shows fluctuations starting from initial time period and stabilizes at $0.6s$. Current waveform shows ripples arise at $0.01s$ and still it continues to reach $0.4s$ and attain $22A$ of current respectively.

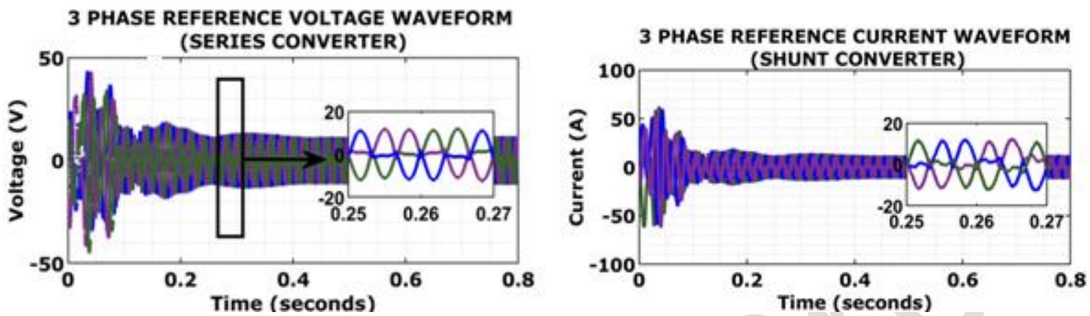

Fig. 14. Reference voltage and current characteristics

Fig. 14 represents series converter voltage showing high-frequency transients initially that stabilize into a steady sinusoidal waveform between 0.25 and 0.27 seconds with a peak amplitude of 20V. Shunt converter displays initial fluctuations that stabilize similarly to the voltage waveform, settling into a steady sinusoidal pattern with a peak amplitude of approximately 20A.

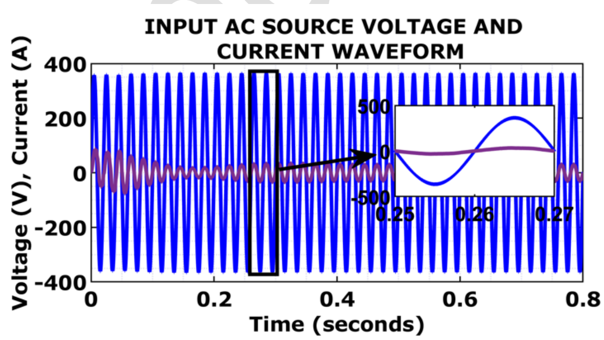

Fig. 15. Input AC source waveform

Fig. 15 represents the input AC source voltage and current waveform. The input AC voltage is the blue sinusoidal line which fluctuates around $350V$. Similarly current is shown in red curve that oscillates from $20A$ and settles at 0.2s.

10.22060/EEJ.2026.25662.5978

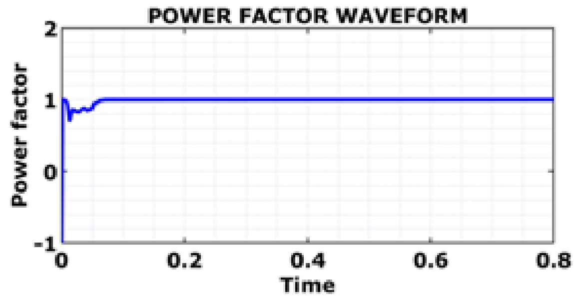

Fig. 16. Power factor (Case 1)

Power factor under case o amplitude is presented in Fig. 16. The waveform of power factor faces more ripples in initial stage and shows unity power factor.

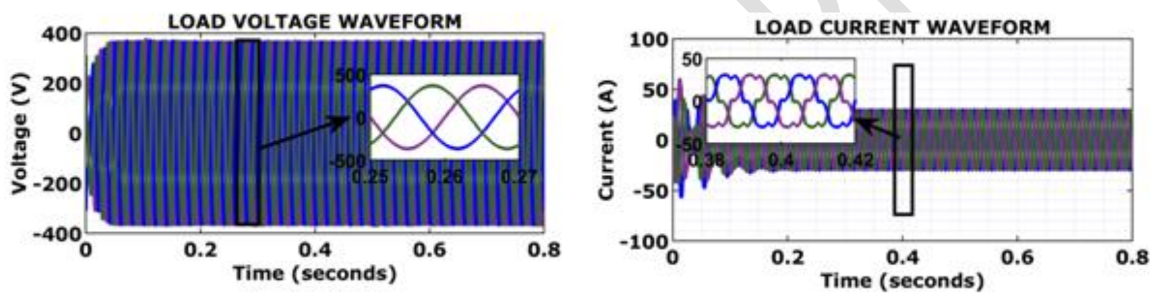

Fig. 17. Load waveform (Case 1)

Fig. 17 shows load voltage and current waveform having oscillations and voltage fluctuates around $400\ to\ -400V$. After 0.25s the voltage becomes stable and the current waveform shows $50\ to\ -50A$ of current.

Case 2) -0.2 Sag

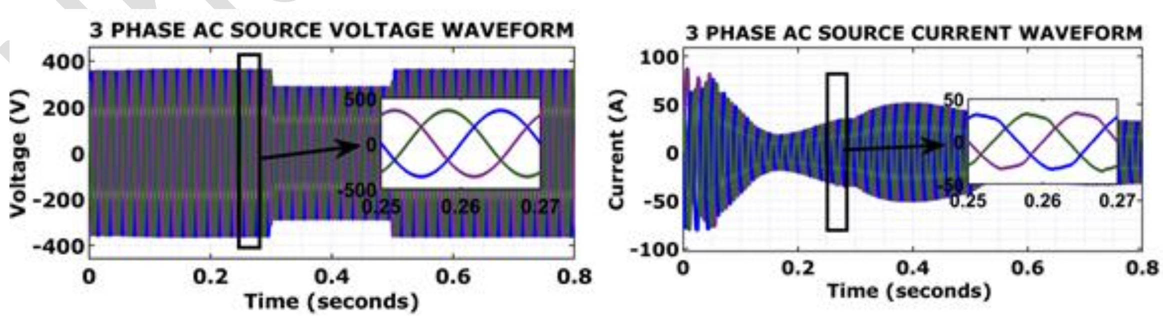

Fig. 18. Three phase AC source waveform (Case 2)

Uncorrected Proof

10.22060/EEJ.2026.25662.5978

Fig. 18 graph shows a AC source voltage waveform with voltage ranging from $-400\,V\;to\;400\,V$. Similarly current ranges from $100to - 100A$. Both the waveform include zoomed-in sections over a time period of 0.8s.

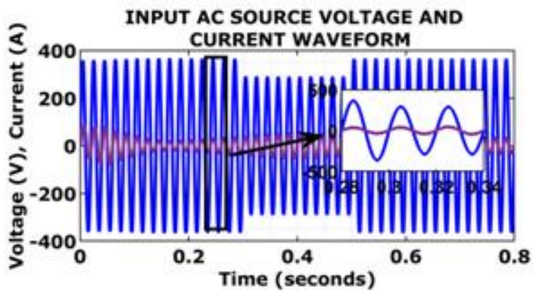

Fig. 19. Input AC source and waveform (Case 2)

The waveform of input AC source and power factor is shown in Fig. 19. The voltage is represented in blue sinusoidal waveform ranging between $-400\,V\;to\;400\,V$.Similarly current waveform oscillates over the entire time period.

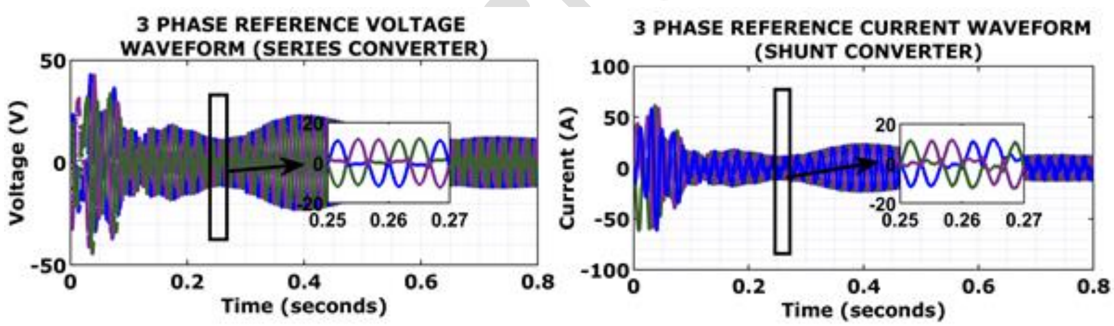

Fig. 20. Three phase reference waveform (Case 2)

The reference voltage and current waveform is revealed in Fig. 20. The reference voltage for series converter is measured in volts and shunt converter provides the reference current measurement. Both the waveform shows the zoomed in sections of 0.25s respectively.

Uncorrected Proof

10.22060/EEJ.2026.25662.5978

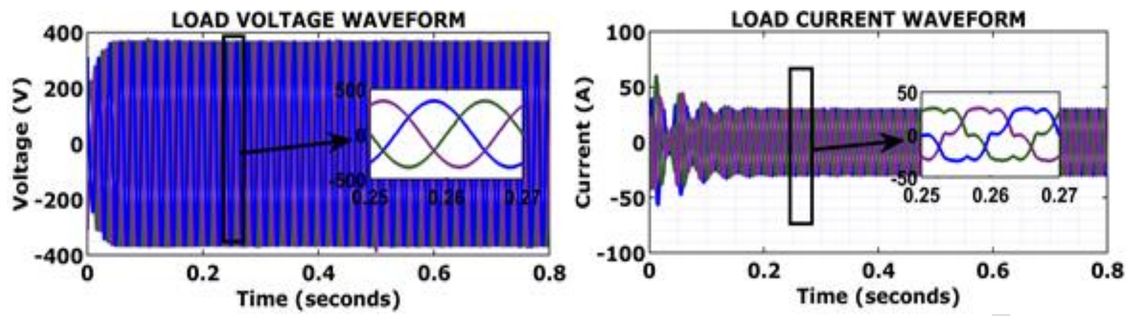

Fig. 21. Load characteristics (Case 2)

The load voltage and current waveform is illustrated in Fig. 21. The load voltage ranges approximately 400 to-400V over 0.8s of time period. Accordingly load current waveform shows $50A$ in a stable sinusoidal representation.

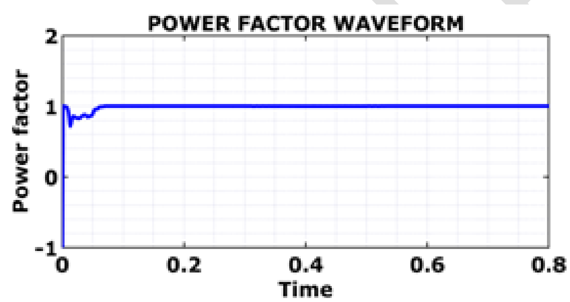

Fig. 22. Power factor waveform (Case 2)

Fig. 22 power factor under case 2. The waveform shows stable power factor value with ripples at initial stage indicating the system has unity power factor.

Case 3) 0.2 Swell

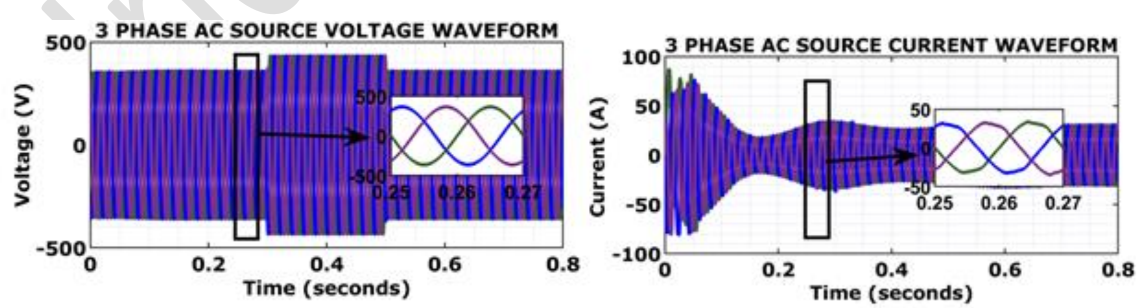

Fig. 23. Three phase AC source waveform (Case 3)

Uncorrected Proof

10.22060/EEJ.2026.25662.5978

An AC source voltage and current is represented in Fig. 23. The voltage ranges around $400 to - 400V$ and at 0.25s the voltage is clearly viewed as sinusoidal form. The current value ranges around $50\ to - 50A$over$0.8s$ respectively.

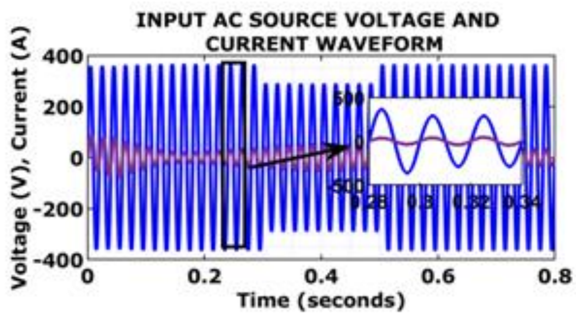

Fig. 24. Input AC source waveform (Case 3)

Input AC source and power factor waveform illustrated in Fig. 24. The AC source waveform highlighting the phase adjustment of voltage and current which is represented in sinusoidal form.

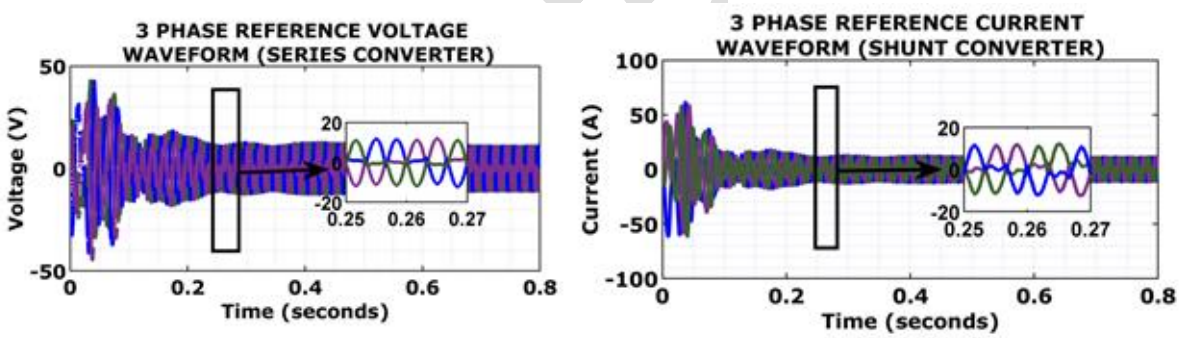

Fig. 25. Three phase reference waveform (Case 3)

The three phase reference characteristics is shown in Fig. 25. The reference voltage is obtained from series converter which fluctuates at $20\ to - 20V$. Similarly reference current waveform shows ripples and after $0.25s$ it becomes stable.

Uncorrected Proof

AUT Journal of Electrical Engineering
10.22060/EEJ.2026.25662.5978

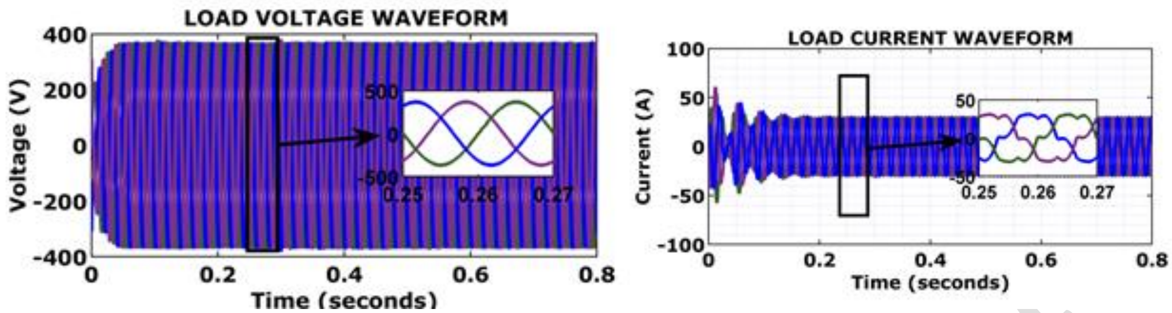

Fig. 26. Load waveform (Case 3)

Fig. 26 demonstrates the load voltage and current waveform. The load voltage oscillates between $400\ to\ -400V$ and the load current fluctuates at $50\ to\ -50A$. Both the waveform shows zoomed in section at $0.25s$ respectively.

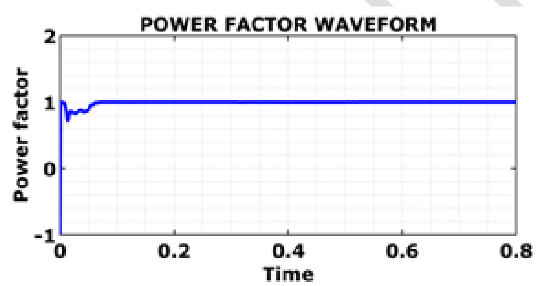

Fig. 27. Power factor waveform (Case 3)

Fig. 27 Power factor waveform. It shows stabilized power factor around unity range indicating the system has better performance.

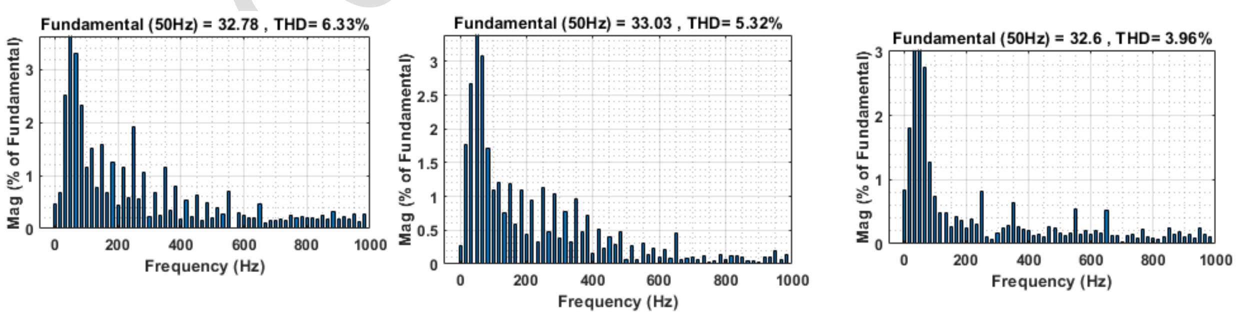

Fig. 28. THD Waveform

corrected Proof

THD for RYB phase is shown in Fig. 28. The R-phase value is obtained 6.33%, where Y-phase has THD of 5.32% and B-phase 3.96% indicating the overall system performs with low amount of harmonic distortion.

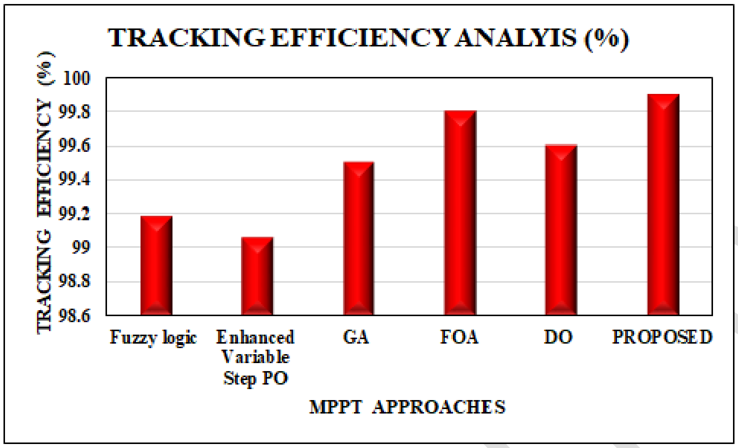

Fig. 29. Tracking efficiency comparison

Tracking efficiency of controllers is illustrated in Fig. 29. The comparison between controllers from ref [13] has 99.1%, in ref [14] the tracking level is 99.06% and the proposed controller achieves 99.9% of greater tracking efficiency while the FOA [25] and DO [26] attains the efficiency of 99.8% and 99.6%.

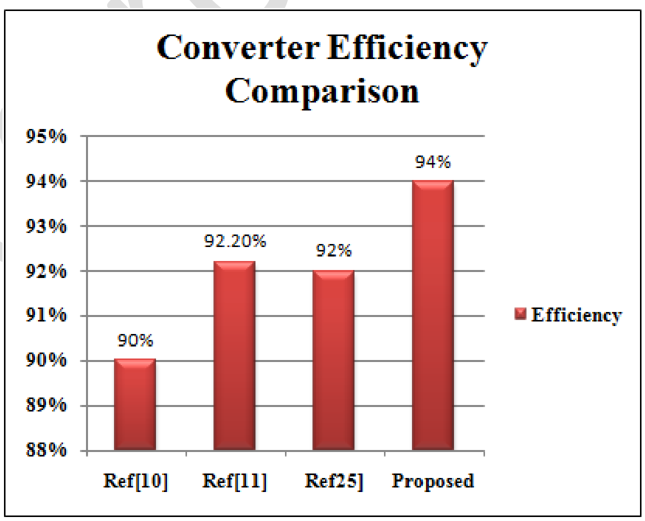

Fig. 30. Efficiency comparison

Uncorrected Proof

The converter efficiency is equated with various converters shown in Fig. 30. Each of converter has achieved as much higher efficiencies as 90% in ref [10], 92% in ref[24], 92.2% in ref [11] while the proposed converter attained 94% of higher efficiency.

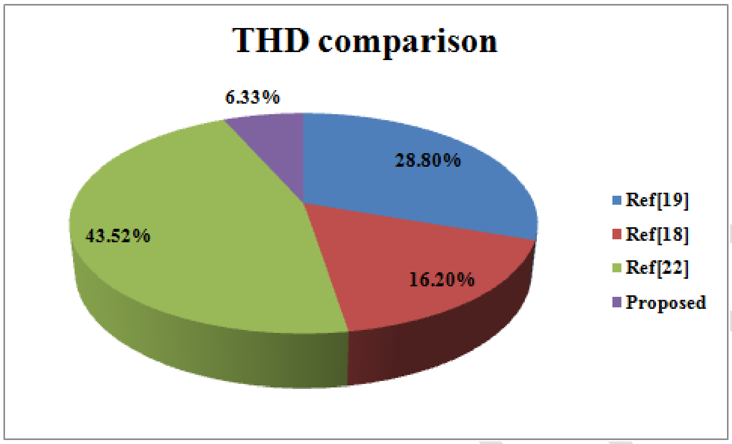

Fig. 31. Comparison of THD

THD comparison between various control strategies is displayed in Fig. 31. THD of proposed converter has the low amount as 6.33% respectively.

Table 2. Power loss comparison

Converter	Power loss
Ref [20]	28.16%
Ref[22]	43.01%
Ref[24]	20.1%
Proposed	0.75%

Table 2 illustrates Power loss in converters compared with various converters. The proposed converter has reduced power loss comparing to other converters in ref [20] [22] and [25] respectively.

Uncorrected Proof

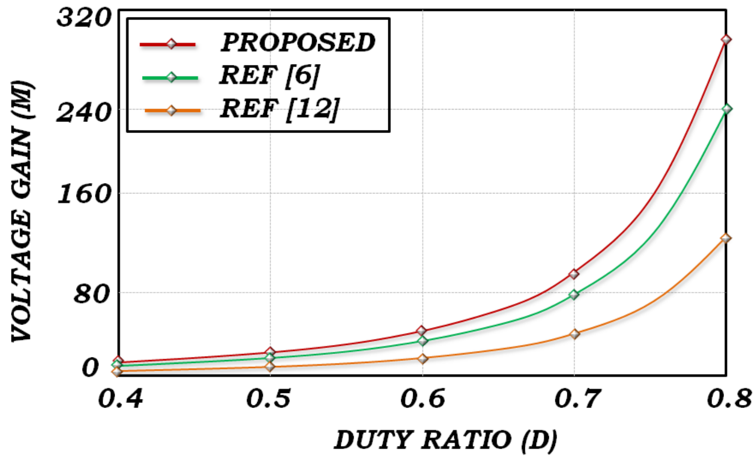

Fig. 32. Voltage gain comparison

Fig. 32 shows voltage gain comparison graph. The comparison is associated between implemented converter and in ref [4] and [12] and finally the implemented converter attains a higher gain.

6. Conclusion

The proposed PV powered based CI active boost step-up converter with an ANN-based MPPT controller using the SFO algorithm. The proposed converter provides efficient step-up capability with improved conversion performance. Meanwhile, the system leverages optimized by SFO-MPPT Controller extract supreme power from PV under fluctuating circumstances. PI controller regulates the DC output voltage while the shunt and series converter maintain voltage stability. Furthermore, the system provides an efficient and integrated solution for managing power flow, offering advantages such as high gain, reduced output ripples, and effective power delivery to the load or grid connection. The experimental results are obtained as converter efficiency of 94%, tracking efficiency 99.9%, THD has reduced to 0.75% of low harmonics respectively. Consequently, this integrated system ensures efficient energy harvesting, stable DC-link voltage regulation and improved power quality.

There is a no hardware prototype implementation or real-time testing under realistic grid conditions is one of the study's main restrictions. Sensor noise, converter losses, communication delays, and environmental

Uncorrected Proof

uncertainties are difficult to precisely represent in simulations affect performance. Nevertheless these drawbacks, the developed approach shows great promise for rising power quality, grid stability and the incorporation of renewable energy in contemporary smart grids. To confirm practical viability, future work should concentrate on real-time implementation and experimental validation on a hardware tested.

References

[1] S. Kumar, and K. Rathore, "Renewable energy for sustainable development goal of clean and affordable energy," International Journal of Materials Manufacturing and Sustainable Technologies, vol. 2, no. 1, pp. 1-15, 2023.

[2] S. Rezaei, A. H. Mejia, Y. Wu, J. Reed, and J. Brouwer, "Global warming impacts of the transition from fossil fuel conversion and infrastructure to hydrogen," Applied Energy, vol. 397, pp. 126363, 2025.

[3] S. Cui, S. Lyu, Y. Ma, and K. Wang, "Improved informer PV power short-term prediction model based on weather typing and AHA-VMD-MPE," Energy, vol. 307, pp. 132766, 2024.

[4] A. Nadermohammadi, P. Abolhassani, A. Seifi, M. Zarrinehbafan, P. Aghakhanlou, S. H. Hosseini, and M. Sabahi, "Cost-effective soft-switching ultra-high step-up DC–DC converter with high power density for DC microgrid application," Scientific Reports, vol. 14, no. 1, pp. 20407, 2024.

[5] A. S. Mansour, and M. S. Zaky, "A new extended single-switch high gain DC–DC boost converter for renewable energy applications," Scientific Reports, vol. 13, no. 1, pp. 264, 2023.

[6] S. Mahdizadeh, H. Gholizadeh, R. S. Shahrivar, E. Afjei, and A. Mosallanejad, "An ultra high step-up DC-DC converter based on VMC, POSLLC, and boost converter," IET Power Electronics, vol. 15, no. 10, pp. 901-918, 2022.

[7] M. A. Samad, Y. Xia, T. Manzoor, K. Mehmood, A. Saleem, A. H. Milyani, and A. A. Azhari, "Composite model predictive control for the boost converter and two-phase interleaved boost converter," Frontiers in Energy Research, vol. 10, pp. 1009812, 2023.

Uncorrected Proof

[8] M. Kumar, and G. Panda, “Analysis of conventional and interleaved boost converter with solar photovoltaic system,” In 2022 International Conference on Intelligent Controller and Computing for Smart Power (ICICCSP), pp. 1-6. IEEE, 2022.

[9] F. Elghabsi, M. R. Sahid, R. Ayop, A. Alanssari, M. Al Takrouri, M. Swadi, M. A. Sahhouk, H. Malik, and V. K. Jadoun, “High gain and high efficiency soft switching quadratic boost converter for renewable energy applications,” Scientific Reports, vol. 15, no. 1, pp. 36238, 2025.

[10] N. Subhani, Z. May, M. K. Alam, I. Khan, M. A. Hossain, and S. Mamun, “An improved non-isolated quadratic DC-DC boost converter with ultra high gain ability,” IEEE Access, vol. 11, pp. 11350-11363, 2023.

[11] D. Rong, X. Chen, and X. Sun, “High gain interleaved dual coupled inductor active quadratic DC-DC converter,” IEEE Access, vol. 12, pp. 76344-76358, 2024.

[12] L. Chen, D. Rong, and X. Sun, “A high-gain interleaved quadric DC-DC converter with dual-coupled inductors,” IEICE Electronics Express, vol. 21, no. 18, pp. 20240408-20240408, 2024.

[13] G. I. Giurgi, L. A. Szolga, and D. V. Giurgi, “Benefits of fuzzy logic on MPPT and PI controllers in the chain of photovoltaic control systems,” Applied Sciences, vol. 12, no. 5, pp. 2318, 2022.

[14] A. Chellakhi, and S. El Beid, “A Real-Time Investigation of an Enhanced Variable Step PO MPPT Controller for Photovoltaic Systems Using dSPACE 1104 Board,” Energies, vol. 18, no. 13, pp. 3343, 2025.

[15] A. Borni, T. Abdelkrim, N. Bouarroudj, A. Bouchakour, L. Zaghba, A. Lakhdari, and L. Zarour, “Optimized MPPT controllers using GA for grid connected photovoltaic systems, comparative study,” Energy Procedia, vol. 119, pp. 278-296, 2017.

[16] M. Naiem-Ur-Rahman, M. M. Hasan, A. M. Raka, M. F. Rahman, M. M. Rana, A. Al Mansur, and M. A. Razzak, “An asymmetric fuzzy-based self-tuned PSO-Optimized MPPT controller for grid-connected solar photovoltaic system,” Energy Conversion and Management: X, vol. 26, pp. 100902, 2025.

Uncorrected Proof

[17] O. Candra, A. Chammam, J. R. N. Alvarez, I. Muda, and H. Ş. Aybar, "The impact of renewable energy sources on the sustainable development of the economy and greenhouse gas emissions," Sustainability, vol. 15, no. 3, pp. 2104, 2023.

[18] A. Gautam, R. Shukla, G. Sudhakar, A. Gautam, V. Pandey, S. Banerjee, and D. De, "Monitoring and Utilization of SVC/STATCOM using SCADA/WAMS in Indian Power system," In 2022 IEEE International Conference on Power Systems Technology (POWERCON), pp. 1-6. IEEE, 2022.

[19] P. V. V. Satyanarayana, A. Radhika, C. R. Reddy, B. Pangedaiah, L. Martirano, A. Massaccesi, A. Flah, and M. Jasiński, "Combined DC-link fed parallel-VSI-based DSTATCOM for power quality improvement of a solar DG integrated system," Electronics, vol. 12, no. 3, pp. 505, 2023.

[20] G. Moustafa, M. Elshahed, A. R. Ginidi, A. M. Shaheen, and H. S. Mansour, "A gradient-based optimizer with a crossover operator for distribution static VAR compensator (D-SVC) sizing and placement in electrical systems," Mathematics, vol. 11, no. 5, pp. 1077, 2023.

[21] N. N. Bon, and T. L. Le, "Application of JAYA algorithm for optimizing allocation and size of thyristor-controlled series compensator devices," Bulletin of Electrical Engineering and Informatics, vol. 14, no. 3, pp. 1647-1655, 2025.

[22] B. E. Elnaghi, A. M. Ismaiel, M. M. Ismail, H. A. Zedan, and A. A. Salem, "Experimental validation of an adaptive fuzzy logic controller for MPPT of grid connected PV system," Scientific Reports, vol. 15, no. 1, pp. 27173, 2025.

[23] A. Bahadori, M. Maalandish, A. Nadermohammadi, and S. H. Hosseini, "A non-isolated DITO high step up DC/DC converter with reduced voltage stress on power switches," Scientific Reports, vol. 15, no. 1, pp. 10163, 2025.

[24] S. J. Chen, S. P. Yang, C. M. Huang, and P. Y. Hu, "High step-up interleaved dc–dc converter with voltage-lift capacitor and voltage multiplier cell," Electronics, vol. 14, no. 6, pp. 1209, 2025.

[25] M. J. Alshareef, "An effective falcon optimization algorithm based MPPT under partial shaded photovoltaic systems." IEEE access, vol.10, pp.131345-131360, 2022.

Uncorrected Proof

10.22060/EEJ.2026.25662.5978

[26] I. Sajid, A. Gautam, A. Sarwar, M. Tariq, H. D. Liu, S. Ahmad, C. H. Lin, A. E. Sayed, "Optimizing photovoltaic power production in partial shading conditions using dandelion optimizer (DO)-based MPPT method." Processes, vol.11, no. 8, pp. 2493, 2023.

Uncorrected Proof